Supplementary Information (SI) for Soft Matter.

Supplementary Notes

Osmotic spawning vesicle

Minoru Kurisu* and Masayuki Imai
Department of Physics, Graduate School of Science, Tohoku University, Japan.

Contents

Supplementary Note 1: Radius change of mother and daughter GUVs.

In addition to **Fig. 2a** and **2b** that show the typical radius changes of a mother GUV (R_{M}) and its daughter GUVs (R_{D}), the results obtained from two further independent observations are shown in **Supplementary Fig. S1a–d**. Binary AOT + Chol (9/1, mol) GUVs prepared in a 20 mM NaH_2PO_4 solution containing 250 mM sucrose were transferred into another 20 mM NaH_2PO_4 solution containing 250 mM fructose (*i.e.*, the typical setup for osmotic spawning). The radii of GUVs were estimated by approximating the vesicle shape as a sphere. The data presented in **Supplementary Fig. S1b** and **1d** were used to generate **Fig. 2c**.

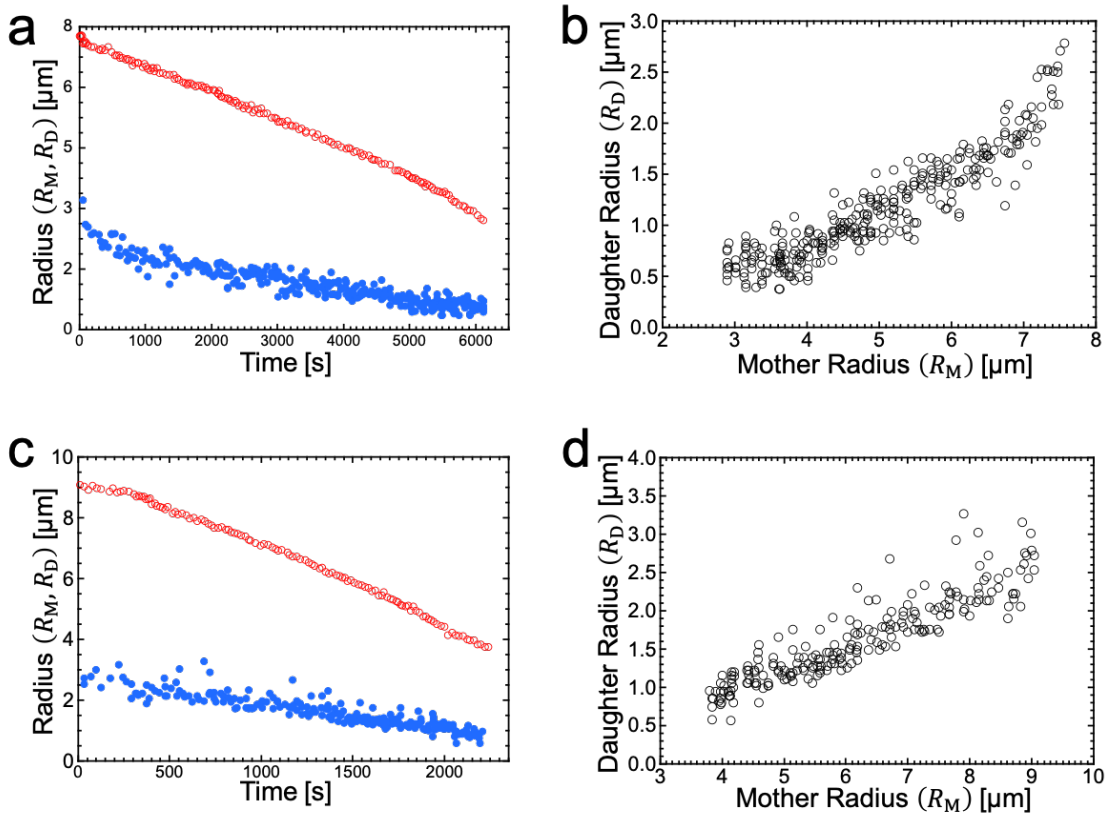

Supplementary Figure S1. Two further independent observations on radius changes of GUVs during osmotic spawning.

(a) Radius change of mother (red open circles) and daughter (blue filled circles) GUVs against time, obtained from a different observation from **Fig. 2a**. The radii of daughter GUVs were measured just after separated from their mother, and thereafter the daughter GUVs gradually increased in size from the plotted values.

(b) Relationship between the radius of mother and daughter GUVs, obtained from **Fig. S1a**.

(c) Radius change of mother and daughter GUVs against time, obtained from a different observation from **Fig. 2a** and **S1a**.

(d) Relationship between the radius of mother and daughter GUVs, obtained from **Fig. S1c**.

Supplementary Note 2: Fusion of two membrane buds.

While a mother GUV spawned about 30–300 daughter GUVs, sometimes two membrane buds were formed on the mother GUV almost simultaneously and then fused into a single membrane bud, resulting in the generation of a larger daughter GUV than the typical size. **Supplementary Fig. S2** presents snapshots of the fusion process. A binary AOT + Chol (9/1, mol) GUV encapsulating a 20 mM NaH_2PO_4 solution containing 250 mM sucrose was transferred into another 20 mM NaH_2PO_4 solution containing 250 mM fructose (*i.e.*, the typical setup for osmotic spawning). Subsequent to the formation of the first membrane bud on the mother GUV (0.0 sec, indicated by a white arrow), the second membrane bud was formed (11.4 sec). The first bud was attracted to and then fused with the second bud while connected to the mother GUV (16.2–19.6 sec), eventually being separated from the mother by spontaneous neck breaking (47.6 sec). The observation of such fusion events provides evidence that the daughter membrane buds appearing on the mother GUVs were connected to the mother membranes via narrow necks, eliminating the possibility that the daughter GUVs, which were generated inside a mother GUV in advance, merely passed through the mother membranes. The larger daughter GUVs produced by this bud fusion behavior are represented as several data points with upward deviations in **Fig. 2c** and downward deviations in **Fig. 2d**.

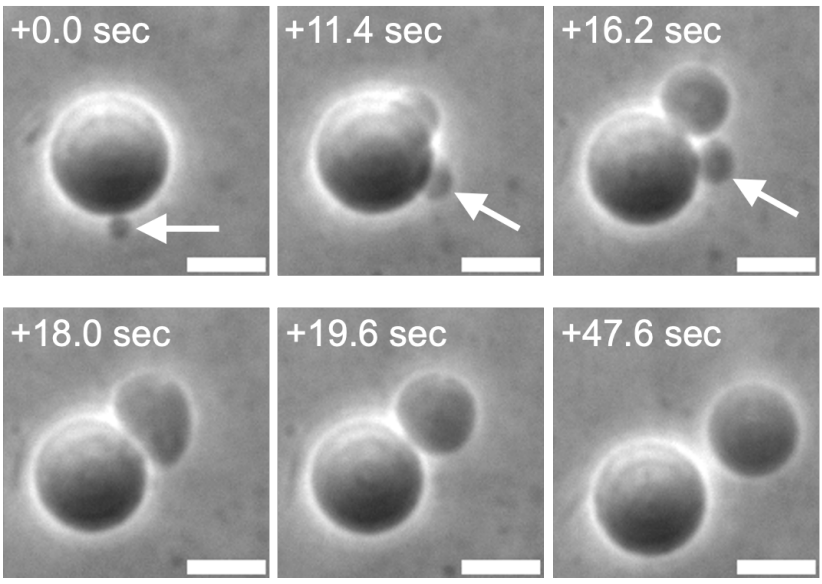

Supplementary Figure S2. Fusion of two buds on a mother GUV.

Phase contrast microscopy images of binary AOT + Chol (9/1) GUVs during osmotic spawning. The images were taken from **Movie S4**. The white arrows indicate the initially formed bud, which moved along the contour of the mother GUV and then fused with the subsequently formed bud. Length of scale bar: 10 μm.

Supplementary Note 3: Asymmetric distribution of Chol between inner and outer monolayers generates spontaneous curvature.

In the osmotic spawning of binary AOT + Chol GUVs, the plausible origin of membrane spontaneous curvature is the asymmetric distribution of Chol between the outer and inner monolayers of vesicle membranes. AOT molecules have a cylindrical shape (*i.e.*, almost zero molecular spontaneous curvature), and Chol molecules have an inverse cone shape (*i.e.*, negative values of molecular spontaneous curvature). The spontaneous curvature of binary AOT + Chol bilayer membranes is expressed by

$$C_0(\equiv 2m) = \frac{1}{2} H_{\mathrm{C}} \Delta\phi_{\mathrm{C}}, \tag{S1}$$

where H_{C} is molecular spontaneous curvature of Chol ($H_{\mathrm{C}} \sim -0.3\ \mathrm{nm}^{-1}$ [S1–S3]), and $\Delta\phi_{\mathrm{C}}$ is the area fraction difference of Chol between the outer and inner monolayers, defined by $\Delta\phi_{\mathrm{C}} = \phi_{\mathrm{C},+} - \phi_{\mathrm{C},-}$ ($\phi_{\mathrm{C},+}$ and $\phi_{\mathrm{C},-}$ are the area fractions of Chol in the outer and inner monolayer, respectively). We assume that AOT and Chol have the same molecular cross-section area a and that the mean area fraction of Chol is $\overline{\phi_{\mathrm{C}}} = \frac{1}{2}\left(\phi_{\mathrm{C},+} + \phi_{\mathrm{C},-}\right) = 0.1$ for binary AOT + Chol (9/1, mol) GUVs. Since Chol has a very fast (milli-seconds) interlayer flip-flop rate [S4] among vesicle-forming amphiphiles, for equilibrated bilayers of the binary GUVs, $\Delta\phi_{\mathrm{C}}$ takes the value which equalizes the chemical potentials of Chol in the outer monolayer ($\mu_{\mathrm{C},+}$) and inner monolayer ($\mu_{\mathrm{C},-}$). Here, the free energy of the outer monolayer of a spherical GUV with radius R and monolayer thickness h is described by the bending energy term and the entropy term as follows [S5,S6]:

$$F_{\mathrm{C},+} = \frac{k_{\mathrm{m}}}{2}\left(\frac{2}{R+\frac{h}{2}} - H_{\mathrm{C}}\phi_{\mathrm{C},+}\right)^2 A_+ + k_{\mathrm{B}}T\left(N_{\mathrm{A},+}\ln\left(1-\phi_{\mathrm{C},+}\right) + N_{\mathrm{C},+}\ln\phi_{\mathrm{C},+}\right), \tag{S2}$$

where k_{m} is monolayer bending rigidity, $N_{\mathrm{A},+}$ and $N_{\mathrm{C},+}$ are the number of molecules of AOT and Chol in the outer monolayer, respectively, $A_+ = (N_{\mathrm{A},+} + N_{\mathrm{C},+})a$ is the outer monolayer area, and area fraction of Chol is expressed as $\phi_{\mathrm{C},+} = N_{\mathrm{C},+}/(N_{\mathrm{A},+} + N_{\mathrm{C},+})$. Then, the chemical potential of Chol in the outer monolayer is given by

$$\mu_{\mathrm{C},+} = \left(\frac{\partial F_{\mathrm{C},+}}{\partial N_{\mathrm{C},+}}\right)_{N_{\mathrm{A},+}} = \frac{k_{\mathrm{m}}a}{2}\left(\frac{2}{R+\frac{h}{2}} - H_{\mathrm{C}}\phi_{\mathrm{C},+}\right)\left(\frac{2}{R+\frac{h}{2}} + H_{\mathrm{C}}\phi_{\mathrm{C},+} - 2H_{\mathrm{C}}\right) + k_{\mathrm{B}}T\ln\phi_{\mathrm{C},+}, \tag{S3}$$

where we apply the typical values of $k_{\mathrm{m}} = 7.5\ k_{\mathrm{B}}T$ (see **Supplementary Note 5**), $h = 1\ \mathrm{nm}$ [S7], and $a = 0.67\ \mathrm{nm}^2$ [S7]. For Chol in the inner monolayer, the chemical potential is similarly given by

$$\mu_{\mathrm{C},-} = \left(\frac{\partial F_{\mathrm{C},-}}{\partial N_{\mathrm{C},-}}\right)_{N_{\mathrm{A},-}} = \frac{k_{\mathrm{m}}a}{2}\left(\frac{2}{R-\frac{h}{2}} + H_{\mathrm{C}}\phi_{\mathrm{C},-}\right)\left(\frac{2}{R-\frac{h}{2}} - H_{\mathrm{C}}\phi_{\mathrm{C},-} + 2H_{\mathrm{C}}\right) + k_{\mathrm{B}}T\ln\phi_{\mathrm{C},-}. \quad \text{(S4)}$$

From the equality of the chemical potentials of Chol (Eqs. (S3) and (S4)), we obtain the equilibrated area fraction difference of Chol $\Delta\phi_{\mathrm{C}}^{\mathrm{eq}} \sim -9.7\cdot10^{-5}$ with the typical radius of mother GUVs $R = 6\ \mu\mathrm{m}$ (**Fig. 2c**), leading to the equilibrated spontaneous curvature of $m^{\mathrm{eq}} \sim 7.2\cdot10^{-3}\mu\mathrm{m}^{-1}$. These values indicate that an equilibrated binary AOT + Chol (9/1) GUV has an almost symmetric Chol distribution in its bilayer and thus the spontaneous curvature of the membrane is insufficient to trigger osmotic spawning (the least required value is estimated as $m_{\mathrm{ini}} \sim \frac{1}{2}\left(R_{\mathrm{M,ini}}^{-1} + R_{\mathrm{D,ini}}^{-1}\right) \sim 0.2\ \mu\mathrm{m}^{-1}$ from **Fig. 2c**). However, during osmotic spawning, AOT molecules in the external solution are inserted into the outer monolayer with the rate of $\delta N_{\mathrm{A},+}^{\mathrm{insert}}/(N_{\mathrm{A},+} + N_{\mathrm{C},+}) \sim 0.1\%\cdot\mathrm{s}^{-1}$ (see **Supplementary Note 4**). Therefore, the balance between the accumulation of AOT in the outer monolayer and the flip-flop transportation of AOT into the inner monolayer will govern the asymmetric distribution of Chol ($\Delta\phi_{\mathrm{C}}$). The value of $\Delta\phi_{\mathrm{C}}$ required to attain $m_{\mathrm{ini}} \sim 0.2\ \mu\mathrm{m}^{-1}$ and to trigger the osmotic spawning is estimated as $\Delta\phi_{\mathrm{C}} = -2.7\cdot10^{-3}$, *i.e.*, Chol distributes only 0.27% more abundant in the inner monolayer. On the other hand, when the spontaneous curvature takes the maximal observed value ($m_{\max} \sim \frac{1}{2}\left(R_{\mathrm{M,min}}^{-1} + R_{\mathrm{D,min}}^{-1}\right) \sim 1.2\ \mu\mathrm{m}^{-1}$, estimated from **Fig. 2c**), the required asymmetric distribution of Chol is estimated as $\Delta\phi_{\mathrm{C}} = -1.6\cdot10^{-2}$ (1.6%), which will compete with the Chol content in the bilayer at the end of osmotic spawning (the initial Chol content $\overline{\phi_{\mathrm{C}}} = 0.1$ is diluted with the spawning progress). The osmotic spawning will end when the required spontaneous curvature becomes hard to be sustained by the molecular insertion in the outer monolayer.

Supplementary Note 4: Insertion rate of amphiphiles from external solution.

During osmotic spawning, mother GUVs incorporate membrane-forming molecules (AOT) from the external solution to relax the tension stress of the vesicle membranes. Here we evaluate the insertion rate of membrane-forming molecules into the outer monolayer of the mother GUVs. We assume that the membrane permeability for disaccharide molecules (sucrose), which are encapsulated by GUVs, is negligibly small compared to that for monosaccharide molecules (fructose). Therefore, the vesicle membranes are treated as impermeable for sucrose. The permeation of fructose into the GUVs is described by [S8]

$$\frac{\mathrm{d}n_{\mathrm{f}}(t)}{\mathrm{d}t} = P_{\mathrm{f}} A_{\mathrm{M}}(t) \left(c_{\mathrm{f}} - \frac{n_{\mathrm{f}}(t)}{V_{\mathrm{M}}(t)} \right), \tag{S5}$$

where n_{f} is the number of fructose molecules encapsulated by a mother GUV, P_{f} is the membrane permeability for sucrose, A_{M} and V_{M} are the surface area and volume of a (mother) GUV, respectively, and c_{f} is the concentration of fructose in the external solution. Since the membrane permeability for water is significantly greater than that for osmolytes, water molecules are assumed to permeate the vesicle membrane instantaneously to cancel the concentration difference of osmolytes across the membrane, namely,

$$\frac{n_{\mathrm{f}}(t) + n_{\mathrm{s}}}{V_{\mathrm{M}}(t)} = c_{\mathrm{f}}\,, \tag{S6}$$

where n_{s} is the number of sucrose molecules (impermeable osmolytes) encapsulated by the GUV that has the initial volume of $V_{\mathrm{M,ini}}$, which is defined by

$$n_{\mathrm{s}} = c_{\mathrm{f}} V_{\mathrm{M,ini}}. \tag{S7}$$

These relations read the osmotic inflation coupled with the asymmetric permeation of osmolytes and the continuous water inflow, described by a derivative form as

$$\frac{\mathrm{d}V_{\mathrm{M}}(t)}{\mathrm{d}t} = P_{\mathrm{f}} A_{\mathrm{M}}(t) \frac{V_{\mathrm{M,ini}}}{V_{\mathrm{M}}(t)}. \tag{S8}$$

This equation is transformed into the derivative equation for the vesicle radius by considering the spherical geometry of the mother GUV as follows:

$$\frac{\mathrm{d}R_{\mathrm{M}}(t)}{\mathrm{d}t} = P_{\mathrm{f}} \left(\frac{R_{\mathrm{M,ini}}}{R_{\mathrm{M}}(t)} \right)^3, \tag{S9}$$

where $R_{\mathrm{M,ini}}$ is the initial radius of the GUV. This derivative equation is solved as

$$R_{\mathrm{M}}(t) = R_{\mathrm{M,ini}} \left(1 + \frac{4 P_{\mathrm{f}}\, t}{R_{\mathrm{M,ini}}} \right)^{\frac{1}{4}} \tag{S10}$$

which describes osmotic inflation and is valid except in the case that the internal sucrose molecules are leaked out, such as by the opening of micro-pores. Assuming that the number of encapsulated sucrose molecules n_{s} decreases to $\varepsilon n_{\mathrm{s}}$ $(0 < \varepsilon < 1)$ per production of a daughter GUV, the radius of the mother GUV between the *n*th and (*n*+1)th productions of

daughter GUVs can be described by correcting Eq. (S10) as follows [S8]:

$$R_{\mathrm{M}}^{(n)}(t) = R_{\mathrm{M,ini}}\left(1 + \varepsilon^n \frac{4P_{\mathrm{f}}\, t}{R_{\mathrm{M,ini}}}\right)^{\frac{1}{4}}. \tag{S11}$$

Therefore, the magnitude of the membrane growth rate for a mother GUV between *n*th and (*n*+1)th daughter GUV production is given by

$$\frac{\mathrm{d}A_{\mathrm{M}}^{(n)}(t)}{\mathrm{d}t} = 8\pi R_{\mathrm{M}}^{(n)}(t)\frac{\mathrm{d}R_{\mathrm{M}}^{(n)}(t)}{\mathrm{d}t} = \frac{8\pi\varepsilon^n P_{\mathrm{f}} R_{\mathrm{M,ini}}}{\sqrt{1 + \varepsilon^n \frac{4P_{\mathrm{f}}\, t}{R_{\mathrm{M,ini}}}}} \sim 8\pi\varepsilon^n P_{\mathrm{f}} R_{\mathrm{M,ini}}\,, \tag{S12}$$

where we used that $P_{\mathrm{f}} \sim 10^{-9}\,\mathrm{m\cdot s^{-1}}$ [S9], $R_{\mathrm{M,ini}} \sim 10^{-5}\,\mathrm{m}$, and $t \sim 10^{3}\,\mathrm{s}$ in the last approximation. This membrane growth is achieved by incorporating vesicle-forming molecules (AOT) from the external solution. Therefore, the magnitude of the molecular insertion rate from the external aqueous solution to the outer monolayer of a mother GUV can be estimated by using Eq. (S12) as follows:

$$\frac{\delta N_{\mathrm{A,+}}^{\mathrm{insert}}}{N_{\mathrm{A,+}} + N_{\mathrm{C,+}}} = \frac{2\cdot\frac{\mathrm{d}A_{\mathrm{M}}^{(n)}}{\mathrm{d}t}}{4\pi R_{\mathrm{M}}^{(n)2}} = \frac{4\varepsilon^n P_{\mathrm{f}}}{R_{\mathrm{M,ini}}\left(1 + \varepsilon^n \frac{4P_{\mathrm{f}}\, t}{R_{\mathrm{M,ini}}}\right)} \sim 4\varepsilon^n \frac{P_{\mathrm{f}}}{R_{\mathrm{M,ini}}}, \tag{S13}$$

where $N_{\mathrm{A,+}}$ and $N_{\mathrm{C,+}}$ are number of AOT and Chol molecules in the outer monolayer of vesicle membranes, respectively. The calculation results in $\sim 10^{-3}\,\mathrm{s^{-1}}$ with the AOT membrane permeability for fructose $P_{\mathrm{f}} = 3\cdot 10^{-9}\,\mathrm{m\cdot s^{-1}}$ [S9], the radius of a mother GUV $R_{\mathrm{M,ini}} = 6\cdot 10^{-6}\,\mathrm{m}$, and the rough value of sucrose loss $\varepsilon^n \sim 0.5$. The distribution of Chol between the outer and inner monolayers will become asymmetric due to this continuous insertion of AOT molecules into the outer monolayer, resulting in the generation of spontaneous curvature on the vesicle membranes (see also **Supplementary Note 3**).

Despite the fast intermonolayer flip-flop motions of Chol [S4] seemingly reducing the asymmetric distribution of Chol, the sustainment of the bilayer asymmetry can be rationalized by the above-mentioned continuous uptake of AOT molecules into the outer monolayer. Here, we consider the number of AOT molecules per unit membrane area in the inner and outer monolayers, $n_{\mathrm{A,-}}$ and $n_{\mathrm{A,+}}$, respectively. Coupling with the uptake of AOT molecules into the outer monolayers and the flip-flop motions in the bilayers, the time evolution of $n_{\mathrm{A,-}}$ and $n_{\mathrm{A,+}}$ can be described as follows [S10]:

$$\frac{\mathrm{d}}{\mathrm{d}t}n_{\mathrm{A,+}}(t) = k\, n_{\mathrm{A,+}}(t) - f_{\mathrm{eff}}\left(n_{\mathrm{A,+}}(t) - n_{\mathrm{A,-}}(t)\right), \tag{S14}$$

$$\frac{\mathrm{d}}{\mathrm{d}t}n_{\mathrm{A,-}}(t) = f_{\mathrm{eff}}\left(n_{\mathrm{A,+}}(t) - n_{\mathrm{A,-}}(t)\right), \tag{S15}$$

where k is the uptake rate of AOT molecules from the external solution into the outer monolayer, and f_{eff} is the effective (*i.e.*, apparent) flip-flop rate of vesicle-forming molecules

(AOT and Chol). These two differential equations read

$$n_{\mathrm{A},+}(t) - n_{\mathrm{A},-}(t) = \frac{k}{2f_{\mathrm{eff}}}\left(1 - \mathrm{e}^{-2f_{\mathrm{eff}}\,t}\right) \xrightarrow{t \to \infty} \frac{k}{2f_{\mathrm{eff}}}. \tag{S16}$$

This outcome rationalizes that the asymmetry of bilayer membranes is sustained by the continuous uptake of AOT molecules (k). Although we cannot address the value of flip-flop rate of AOT (presumably slower than that of Chol), the small value of bilayer asymmetry required to trigger osmotic spawning (only ~$3 \cdot 10^{-3}$; **Supplementary Note 3**) is plausibly generated even in the presence of fast flip-flop motions (f_{eff}).

Supplementary Note 5: Bending rigidity measurement of binary AOT + Chol (9/1) membranes.

Since there were no reports on the bending rigidity of binary AOT + Chol membranes, we measured the value by using the fluctuation spectroscopy [S11–S13] (see also **Method**). First, membrane fluctuations of quasi-spherical GUVs were recorded by phase-contrast microscopy, and the vesicle contours were detected for the sequences of 3000–4000 snapshots per GUV (**Supplementary Fig. S3a**). Then, the angler correlation function of fluctuating vesicle contour $\Xi(\gamma,t) = 1/(2\pi R_0^2)\int_0^{2\pi} \mathrm{d}\phi\,[R(\gamma+\phi,t)\cdot R(\gamma,t)]$, where R is the distance from the centre of vesicle to the contour position at angle γ and at time t, R_0 is the mean radius, and ϕ is the angle by which two positions at vesicle contour are separated, was obtained from each snapshot. The ensemble (time) average $\langle\Xi(\gamma)\rangle = (1/t_1)\int_0^{t_1}\mathrm{d}t'\,\Xi(\gamma,t')$ for each quasi-spherical GUV contains general information about the process governing membrane-shape fluctuations (**Supplementary Fig. S3b**). Here, by using the Legendre polynomial transformation for each contour $\xi_l(t) = (l+1/2)\int_{-1}^{1}\mathrm{d}\cos(\gamma)\;\Xi(\gamma,t)P_l(\cos(\gamma))$, where $P_l(x)$ is the Legendre polynomial, the averaged correlation function was decomposed by $\langle\xi_l\rangle$ to the form of $\langle\Xi(\gamma)\rangle = \sum_l\langle\xi_l\rangle\,P_l(\cos(\gamma))$. The ensemble (time) average of ξ_l obtained from $\langle\Xi(\gamma)\rangle$ decays against Legendre mode l as shown in **Supplementary Fig. 3c**, which can be fitted by

$$\langle\xi_l\rangle = \frac{k_\mathrm{B}T}{4\pi}\frac{2l+1}{\kappa(l-1)(l+2)\left(l(l+1)+\tilde{\Sigma}\right)} \quad (l\geq 2), \tag{S17}$$

where membrane bending rigidity κ and reduced tension $\tilde{\Sigma}$ are fitting parameters.

The κ values obtained from several binary AOT + Chol (9/1) GUVs and several DOPC GUVs (for reference) are summarized in **Supplementary Table 1**. It should be noted that the membrane fluctuations of binary AOT + Chol GUVs were recorded by using 20 mM NaH_2PO_4 solution containing 250 mM sucrose as the internal solution and 20 mM NaH_2PO_4 solution containing 275 mM fructose as the external solution for creating a distinct contrast at vesicle contour and for decreasing the influence from membrane tension $\tilde{\Sigma}$ by draining some water from the GUVs. For the observations of DOPC GUVs, 250 mM sucrose and 275 mM fructose solution were used (*i.e.*, no NaH_2PO_4 contained) as the internal and external solution, respectively. As a reference measurement, the bilayer bending rigidity of DOPC membranes was measured to be $\kappa_\mathrm{DOPC} = 30.0 \pm 2.3\,k_\mathrm{B}T$ from four independent observations, which agrees with the previously reported values by using fluctuation spectroscopy [S12]. Thus, the bilayer bending rigidity of binary AOT + Chol (9/1, mol) membranes was successfully measured as $\kappa_\mathrm{AOT+Chol} = 14.7 \pm 1.8\,k_\mathrm{B}T$ from six independent observations.

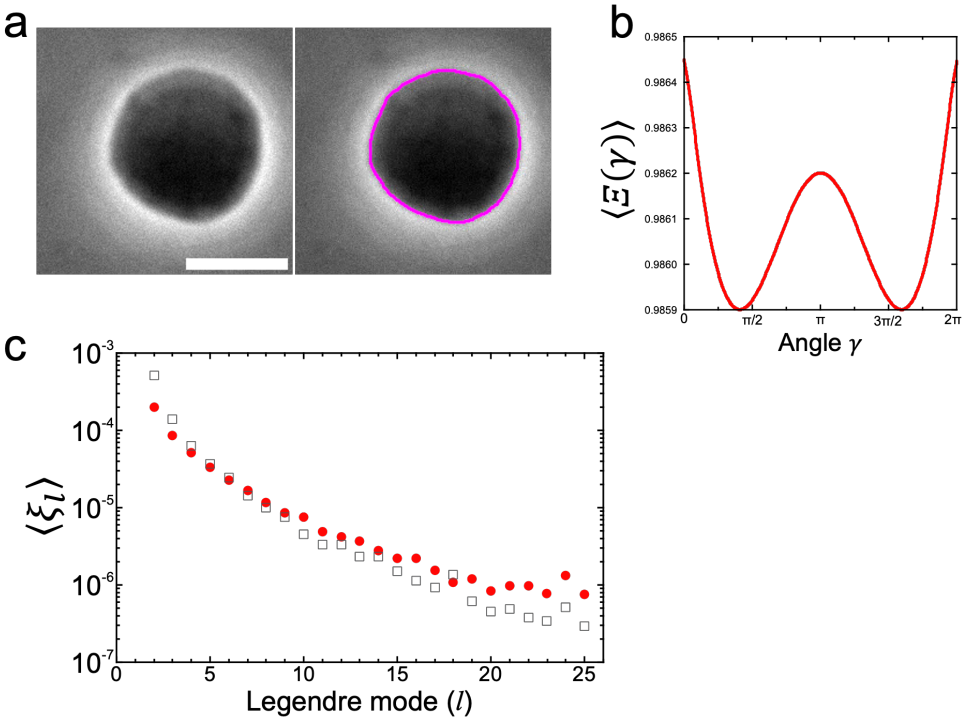

Supplementary Figure S3. Analytical process in fluctuation spectroscopy.

(a) Phase contrast microscopy image of a binary AOT + Chol (9/1) GUV with a fluctuating membrane contour (left) and the result of contour detection (right). Snapshots were recorded at an exposure time of 0.25 ms. Length of scale bar: 10 μm.

(b) Ensemble (time) average of angular correlation function $\Xi(\gamma, t)$ obtained from a sequence of 3668 contours of a fluctuating binary AOT + Chol (9/1) GUV.

(c) Legendre polynomial decompositions of $\langle \Xi(\gamma) \rangle$ for a binary AOT + Chol (9/1) GUV (red filled circles) and for a DOPC GUV (black open squares).

Supplementary Table 1. Obtained bilayer bending rigidity values.

Each data number represents an independent measurement of a single GUV.

No.	Membrane	κ [$k_B T$]	Fitting Error [$k_B T$]
1	DOPC	30.52	± 1.27
2	DOPC	28.41	± 3.74
3	DOPC	32.97	± 1.10
4	DOPC	28.11	± 1.25
5	AOT+Chol (9/1)	13.77	± 0.49
6	AOT+Chol (9/1)	12.87	± 0.72
7	AOT+Chol (9/1)	16.37	± 1.42
8	AOT+Chol (9/1)	15.89	± 1.52
9	AOT+Chol (9/1)	12.65	± 0.88
10	AOT+Chol (9/1)	16.75	± 0.82

Supplementary Note 6: Descriptions of the supplementary movies.

Supplementary Movie S1: Original movie of Fig. 1b.

Phase contrast light microscopy movie of a binary AOT + Chol (9/1, mol) GUV during osmotic spawning. A small volume of aqueous solution (pH = 4.3) containing 20 mM NaH_2PO_4, 250 mM sucrose, and a few binary AOT + Chol GUVs was transferred into another aqueous solution (pH = 4.3) containing 20 mM NaH_2PO_4, 250 mM fructose, and 3.0 mM AOT (see **Methods**). The recording of a target mother GUV was initiated a few tens of seconds after the transfer. The mother GUV exhibited a repeated spawning of daughter GUVs, accompanied by a gradual decrease in radius. Selected snapshots are shown in **Fig. 1b**. The elapsed time after starting the recording is indicated at the upper left of the movie. Length of scale bar: 10 μm.

Supplementary Movie S2: Additional movie of an osmotic spawning GUV.

Phase contrast light microscopy movie of a different AOT + Chol (9/1) GUV under the same experimental setup with **Movie S1**.

Supplementary Movie S3: Original movie file for Fig. 1e.

Phase contrast light microscopy movie of the identical AOT + Chol (9/1) GUV to that shown in **Movie S1**, exhibiting the end of osmotic spawning without time compression. A membrane bud formed on the mother GUV increased in radius nearly to that of the mother GUV and was finally fused with the mother GUV. The elapsed time is indicated at the upper left of the movie. Length of scale bar: 5 μm.

Supplementary Movie S4: Original movie of Supplementary Fig. S2.

Phase contrast light microscopy movie of the fusion of two membrane buds on a mother AOT + Chol (9/1) GUV. The experimental setup is the same as **Movie S1**. Selected snapshots are shown in **Supplementary Fig. S2**. The elapsed time is indicated at the upper left of the movie. Length of scale bar: 10 μm.

Supplementary Movie S5: Original movie of Fig. 7.

Phase contrast light microscopy movie of the unsuccessful spawning observed by using high-permeability molecules (glycerol) as the external osmolyte. A small volume of aqueous solution (pH = 4.3) containing 20 mM NaH_2PO_4, 250 mM sucrose, and a few binary AOT + Chol GUVs was transferred into another aqueous solution (pH = 4.3) containing 20 mM NaH_2PO_4, 250 mM glycerol (~10^2 times higher permeability than fructose), and 3.0 mM

AOT. The recording of a target GUV was initiated a few tens of seconds after the transfer. Selected snapshots are shown in **Fig. 7**. The elapsed time after starting the recording is indicated at the upper left of the movie. Length of scale bar: 10 μm.

References

S1 J. Zimmerberg and M. M. Kozlov, *Nat. Rev. Mol. Cell Biol.*, 2006, **7**, 9–19.

S2 Z. Chen and R. P. Rand, *Biophys. J.*, 1997, **73**, 267–276.

S3 M. Imai, Y. Sakuma, M. Kurisu and P. Walde, *Soft Matter*, 2022, **18**, 4823–4849.

S4 J. A. Hamilton, *Curr. Opin. Lipidol.*, 2003, **14**, 263–271.

S5 J. Derganc, *Phys. Biol.*, 2007, **4**, 317–324.

S6 A. Tian and T. Baumgart, *Biophys. J.*, 2009, **96**, 2676–2688.

S7 I. Grillo, P. Levitz and T. Zemb, *Langmuir*, 2000, **16**, 4830–4839.

S8 M. Mally, P. Peterlin and S. Svetina, *J. Phys. Chem. B*, 2013, **117**, 12086–12094.

S9 M. Kurisu, R. Katayama, Y. Sakuma, T. Kawakatsu, P. Walde and M. Imai, *Commun. Chem.*, 2023, **6**, 56.

S10 M. Nakano, M. Fukuda, T. Kudo, H. Endo and T. Handa, *Phys. Rev. Lett.*, 2007, **98**, 30–33.

S11 J.H. Ipsen, A.G. Hansen and T. Bhatia, In *The Giant Vesicle Book*, eds. R. Dimova and C.M. Marques, CRC Press, Boca Raton, 2020, Chapter 14: Vesicle fluctuation analysis, 333–345.

S12 H. A. Faizi, C. J. Reeves, V. N. Georgiev, P. M. Vlahovska and R. Dimova, *Soft Matter*, 2020, **16**, 8996–9001.

S13 J. F. Faucon, M. D. Mitov, P. Méléard, I. Bivas and P. Bothorel, *J. Phys. Fr.*, 1989, **50**, 2389–2414.